



V.V. Lysko

V.V. Lysko, *Cand.Sc (Phys-Math)*^{1,2}
O.V. Nitsovich, *Cand.Sc (Phys-Math)*^{1,2}



O.V. Nitsovich

¹Institute of Thermoelectricity of the NAS
and MES of Ukraine,
1, Nauky str., Chernivtsi, 58029, Ukraine;
²Yuriy Fedkovych Chernivtsi National University,
2, Kotsiubynsky str., Chernivtsi, 58012, Ukraine
e-mail: anatykh@gmail.com

COMPUTER OPTIMIZATION OF THE VERTICAL ZONE MELTING METHOD FOR MANUFACTURING FLAT INGOTS OF THERMOELECTRIC MATERIALS BASED ON Bi_2Te_3

The results of computer simulation of the process of manufacturing flat ingots of thermoelectric materials based on Bi_2Te_3 by the method of vertical zone melting are presented. The dependences of the crystallization front shape on the geometric dimensions of the heater and coolers, their temperatures, speed of movement and other process parameters are given. Multifactor computer optimization of process modes and equipment design for growing flat ingots of thermoelectric materials based on Bi_2Te_3 is carried out. Bibl. 20, Figs. 14.

Key words: simulation, vertical zone melting, thermoelectric material, bismuth telluride.

Introduction

Thermoelectricity is finding more and more practical applications in various industries. According to estimates [1], the thermoelectric product market today is more than 800 million US dollars and is growing annually by approximately 9%. More than 55 million thermoelectric modules are produced. At the same time, thermoelectric materials based on *Bi-Te* remain the main ones in production.

Self-contained thermoelectric power sources operating from the heat of combustion of any fuel are especially promising and can be used as autonomous low-power power sources for powering equipment for various purposes. They have a long service life, are highly reliable and resistant to climatic and impact loads, are universal, silent in operation and easy to use. Scientists and engineers of many countries are actively working on the creation of such sources. Thermoelectric generators with an electric power of 2 – 20 W designed for charging mobile phones, MP3 players, navigators during trips and tourist trips were developed by a number of foreign companies (TES, Power Pot, Biolite) [2 – 7]. Thermoelectric generators have also been developed, the operation of which is based on the use of heat from solid fuel furnaces [8 – 10]. They are serially produced by a number of enterprises [10 – 12]. At the same time, the main obstacle for their widespread practical use is a relatively high cost, primarily due to the high cost of the thermoelectric material from which they are made. Therefore, a lot of attention is paid to the improvement of methods of obtaining thermoelectric materials based on *Bi-Te* [13 – 18].

One of the possibilities for reducing the cost of the material and decreasing the technological defects when cutting ingots into thermoelements is the production of ingots in the form of flat rods. The creation of a technology for the production of such ingots requires multi-parameter optimization of the

controlled parameters of the growing process.

The work [19] shows the results of creating a computer model of the process of manufacturing flat ingots of thermoelectric materials by the method of vertical zone melting, which is one of the most common industrial methods of growing polycrystalline thermoelectric materials based on $Bi-Te$.

The purpose of this work is multifactorial computer optimization of technological modes and design of equipment for the production of flat ingots of thermoelectric materials based on Bi_2Te_3 .

1. Physical, mathematical and computer models of vertical zone melting process

The quality of thermoelectric material obtained by vertical zone melting is affected by various factors, such as: impurity distribution coefficient; length of the molten zone; zone movement speed; degree of mixing of the molten zone; heater temperature, etc. The main technological characteristic of growth is the curvature of the crystallization front, determined by the values of the radial and axial temperature gradients in the ingot during growth.

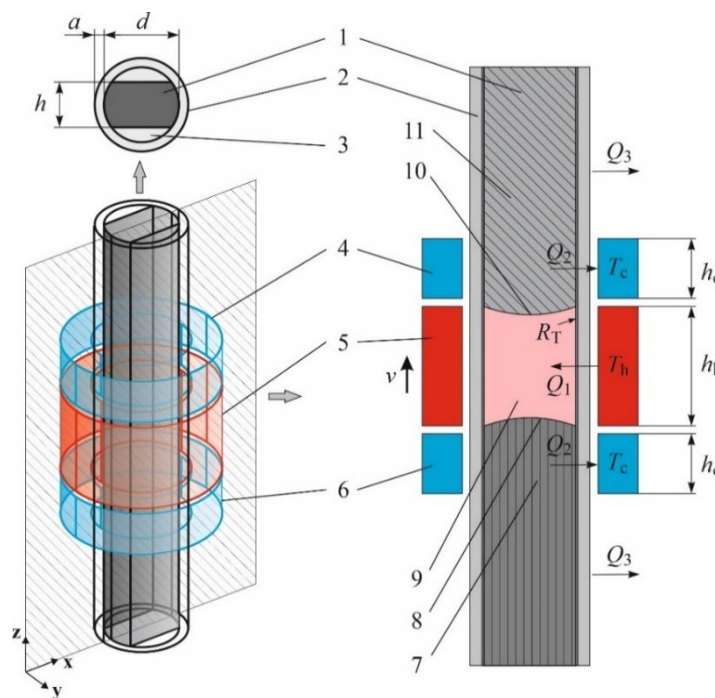


Fig. 1. Physical model of growing thermoelectric materials by vertical zone melting: 1 – thermoelectric material; 2 – container; 3 – quartz inserts; 4, 6 – coolers; 5 – heater; 7 – material in solid phase (structurally oriented crystal); 8 – crystallization front; 9 – melt zone; 10 – melt front; 11 – material in solid phase (polycrystal).

The shape of the crystallization front can be convex in the liquid phase, flat or concave in the solid phase. The most favorable for growing single crystals with a low density of defects is a flat crystallization front. To create a computer model of the process of growing flat ingots of thermoelectric materials based on Bi_2Te_3 , which allows us to study the dependence of the crystallization front shape on various technological parameters, a physical model was constructed, shown in Fig. 1. The figure shows a fragment of an ingot, which includes polycrystalline material 11, a molten zone 9 and a single crystal 7. The ingot is placed in a container 2. With the help of a heater 5 and a system of coolers 4 and 6, a molten zone 9 is formed, which, moving together with the heater along the ingot, ensures the melting of

the polycrystal and the crystallization of the melt below the boundary 8, which is called the crystallization front.

The COMSOL Multiphysics package of application programs [20] was used for computer simulation of the process of growing Bi_2Te_3 thermoelectric material.

The temperature distribution in the sample under study consists of the solution of the differential equation of thermal conductivity, supplemented by the dependencies of the physical properties of the material under study, as a function of the phase state at a given point at a given temperature:

$$\rho C_p \frac{\partial T}{\partial t} + \rho C_p u \nabla T + \nabla q = Q, \quad (1)$$

$$q = -\kappa \nabla T, \quad (2)$$

$$\rho = \theta \rho_{phase1} + (1 - \theta) \rho_{phase2}, \quad (3)$$

$$C_p = \frac{1}{2} \left(\theta \rho_{phase1} C_{p_{phase1}} + (1 - \theta) \rho_{phase2} C_{p_{phase2}} \right) + L \frac{d\alpha_m}{dT}, \quad (4)$$

$$\alpha_m = \frac{1}{2} \cdot \frac{(1-\theta)\rho_{phase2} - \theta\rho_{phase1}}{\theta\rho_{phase1} + (1-\theta)\rho_{phase2}}, \quad (5)$$

$$\kappa = \theta \kappa_{phase1} + (1 - \theta) \kappa_{phase2}, \quad (6)$$

where ρ is the density, C_p is the heat capacity of the material, κ is the thermal conductivity, u is the velocity of the medium which is zero in the problem under study, T is the temperature, θ is the phase ratio at a given temperature, α_m is the mass ratio between the phases, L is the latent heat of the phase transition, Q is the external heat flow. The *phase1* and *phase2* indices indicate which phase the properties belong to, the solid phase or the liquid phase, respectively.

When modeling zone melting, a stationary mode was considered, i.e. the movement of the thermal unit, including the heater and coolers, was not taken into account. It is known that bismuth telluride-based crystals are grown at a rate of 1.5 – 2.5 cm/hour. Having estimated the time required for the system to achieve thermal equilibrium, it was determined that during this time the heater would shift less than 0.2 mm. Heat loss in this area will be two orders of magnitude less than the heat transmitted from the thermal unit to the ampoule. Thus, these losses can be neglected in computer simulations, as they will have little effect on the overall temperature distribution.

For calculations in the created computer model, the geometric dimensions of the system elements, the temperatures of the heater and coolers, the liquidus and solidus temperatures of the thermoelectric material based on Bi_2Te_3 , as well as the temperature dependences of the properties of the grown material are specified.

2. Results of computer optimization

Fig. 2 shows an example of the crystallization front shape obtained by simulation using the method described above for the case of a flat Bi_2Te_3 ingot with a thickness of 12 mm, a container diameter of $d = 24$ mm, a heater height of $h_h = 72$ mm, and a cooler height of $h_c = 24$ mm (the heater height is 3d, the cooler height is 1d), a heater temperature $T_h = 760$ °C, and a cooler temperature $T_c = 30$ °C.

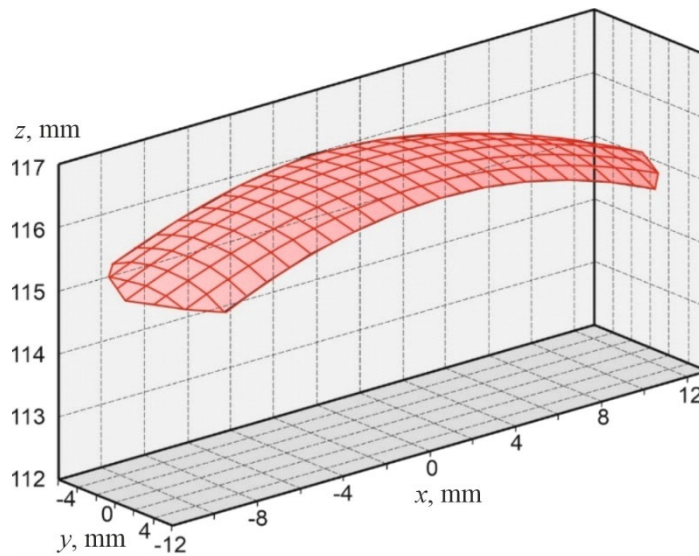


Fig. 2. Example of the shape of crystallization front (for a flat ingot with a thickness $h = 12$ mm, container diameter $d = 24$ mm, heater height $h_h = 72$ mm and cooler height $h_c = 24$ mm, heater temperature $T_h = 760^\circ\text{C}$).

The shape of crystallization front in sections YZ ($x = 0$) and XZ ($y = 0$) at different sizes of the ingot, heater, and coolers, as well as at different temperatures of the heater, is shown in Figs. 3 – 13.

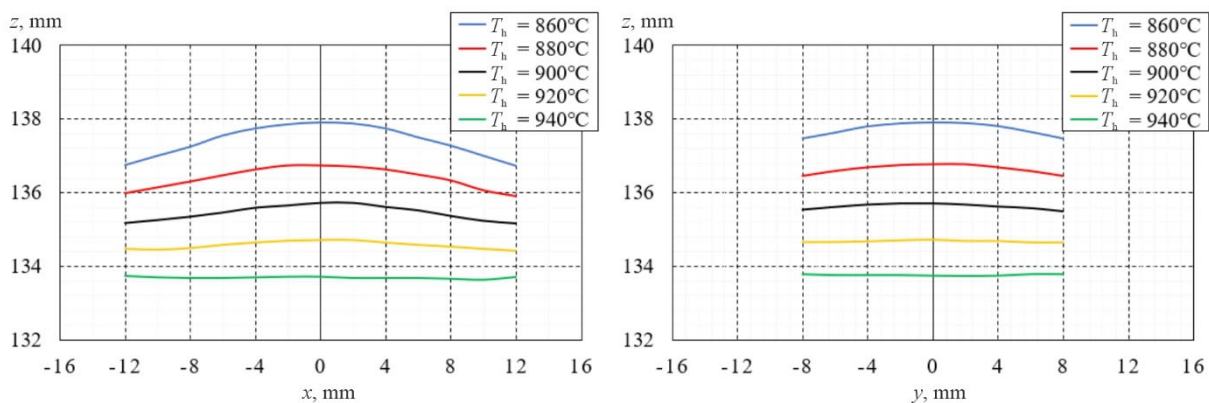


Fig. 3. The shape of crystallization front in sections XZ ($y = 0$) and YZ ($x = 0$) for different temperatures of the heater T_h (with ingot thickness $h = 16$ mm, container diameter $d = 24$ mm, heater height $h_h = 1d = 24$ mm, cooler height $h_c = 1d = 24$ mm).

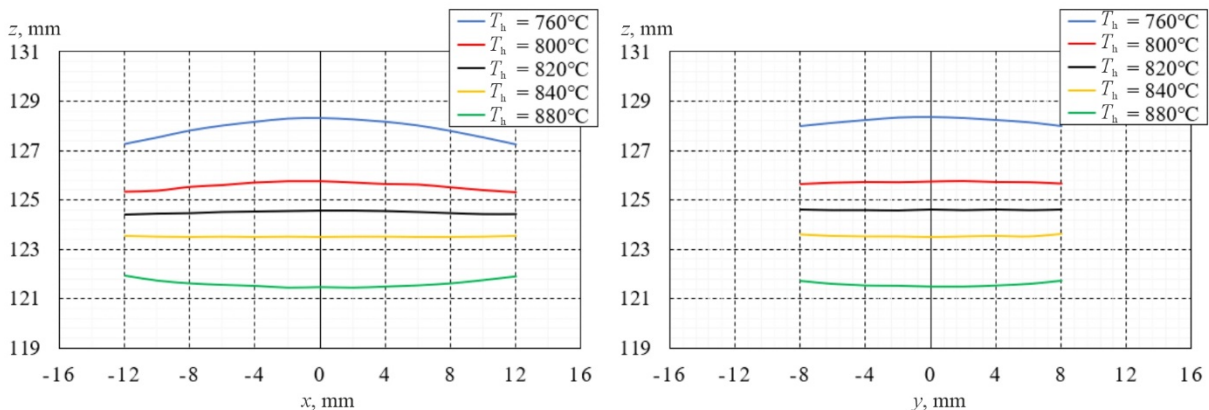


Fig. 4. The shape of crystallization front in sections XZ ($y = 0$) and YZ ($x = 0$) for different temperatures of the heater T_h (with ingot thickness $h = 16$ mm, container diameter $d = 24$ mm, heater height $h_h = 2d = 48$ mm, cooler height $h_c = 1d = 24$ mm).

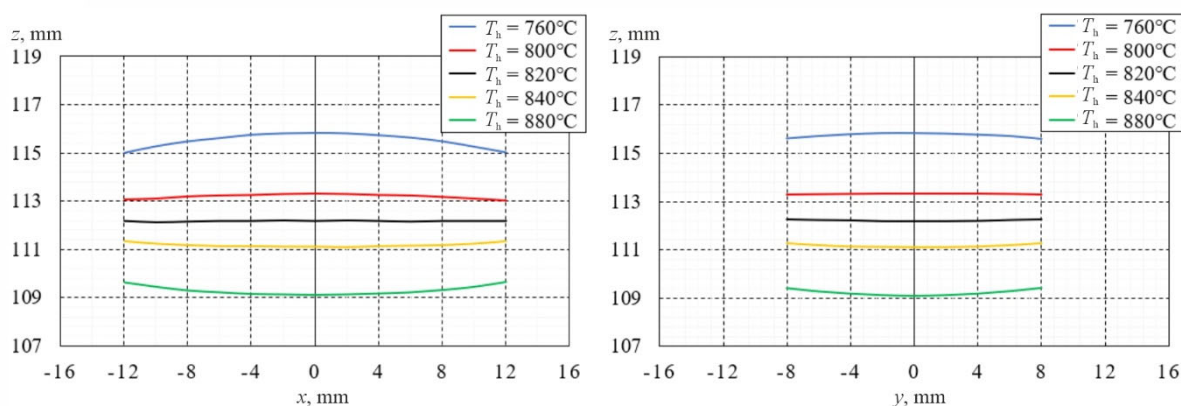


Fig. 5. The shape of crystallization front in sections XZ ($y = 0$) and YZ ($x = 0$) for different temperatures of the heater T_h (with ingot thickness $h = 16$ mm, container diameter $d = 24$ mm, heater height $h_h = 3d = 72$ mm, cooler height $h_c = 1d = 24$ mm).

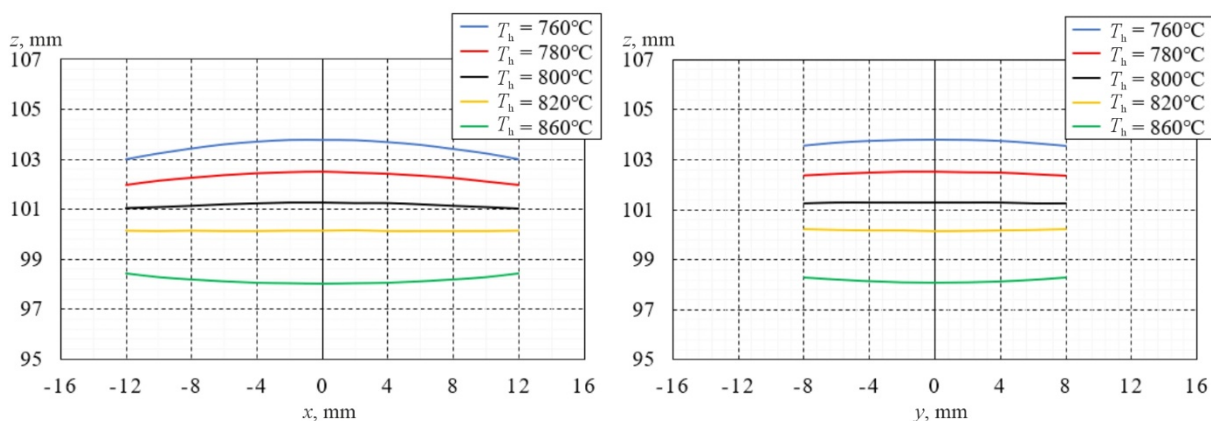


Fig. 6. The shape of crystallization front in sections XZ ($y = 0$) and YZ ($x = 0$) for different temperatures of the heater T_h (with ingot thickness $h = 16$ mm, container diameter $d = 24$ mm, heater height $h_h = 4d = 96$ mm, cooler height $h_c = 1d = 24$ mm).

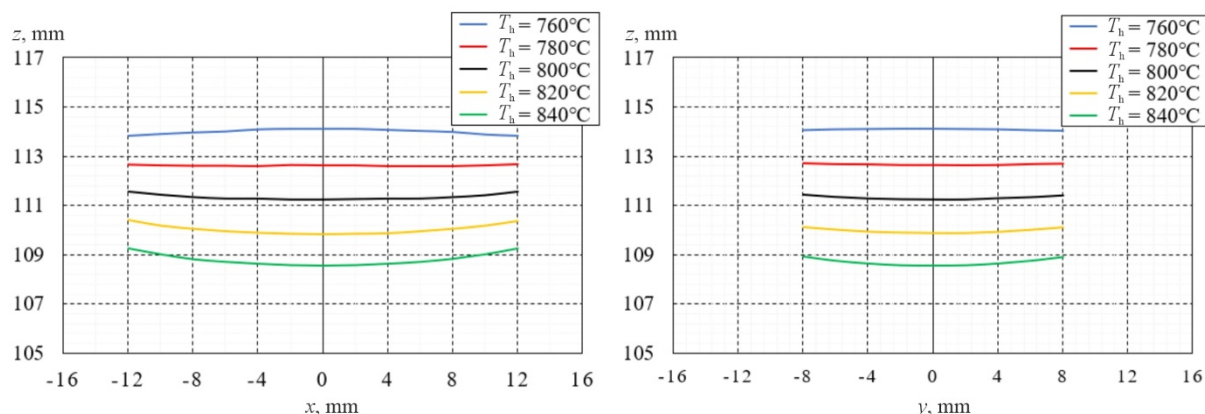


Fig. 7. The shape of crystallization front in sections XZ ($y = 0$) and YZ ($x = 0$) for different heater temperatures T_h (with ingot thickness $h = 16$ mm, container diameter $d = 24$ mm, heater height $h_h = 3d = 72$ mm, cooler height $h_c = 0.25d = 6$ mm).

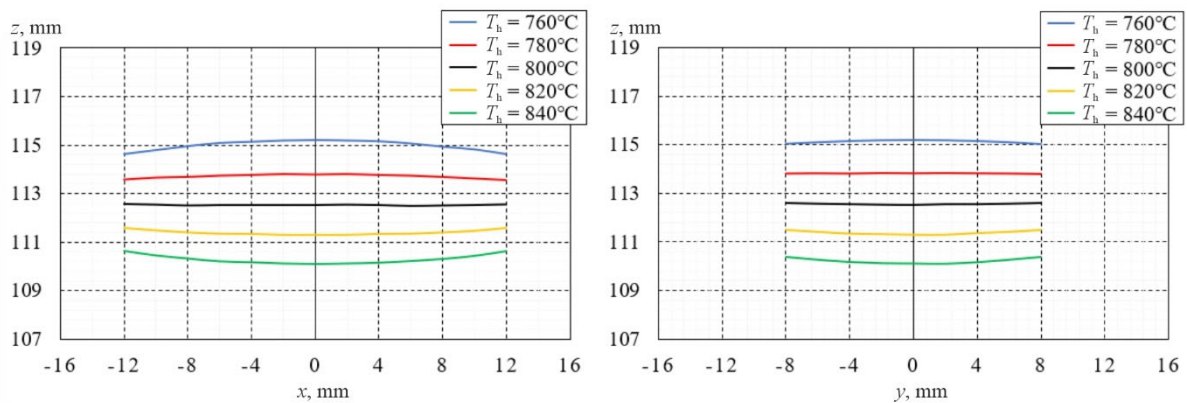


Fig. 8. The shape of crystallization front in sections XZ ($y = 0$) and YZ ($x = 0$) for different heater temperatures T_h (with ingot thickness $h = 16$ mm, container diameter $d = 24$ mm, heater height $h_h = 3d = 72$ mm, cooler height $h_c = 0.5d = 12$ mm).

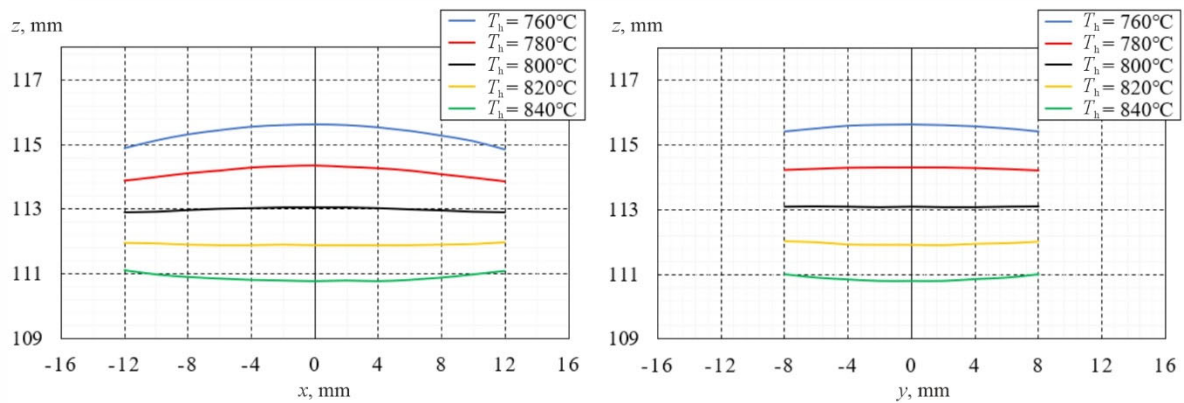


Fig. 9. The shape of crystallization front in sections XZ ($y = 0$) and YZ ($x = 0$) for different heater temperatures T_h (with ingot thickness $h = 16$ mm, container diameter $d = 24$ mm, heater height $h_h = 3d = 72$ mm, cooler height $h_c = 0.75d = 18$ mm).

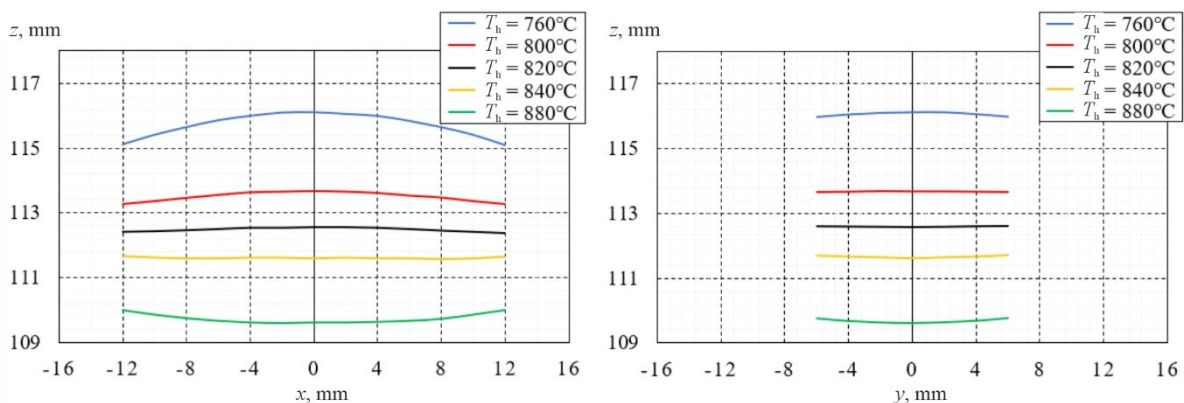


Fig. 10. The shape of crystallization front in sections XZ ($y = 0$) and YZ ($x = 0$) for different heater temperatures T_h (with ingot thickness $h = 12$ mm, container diameter $d = 24$ mm, heater height $h_h = 3d = 72$ mm, cooler height $h_c = 1d = 24$ mm).

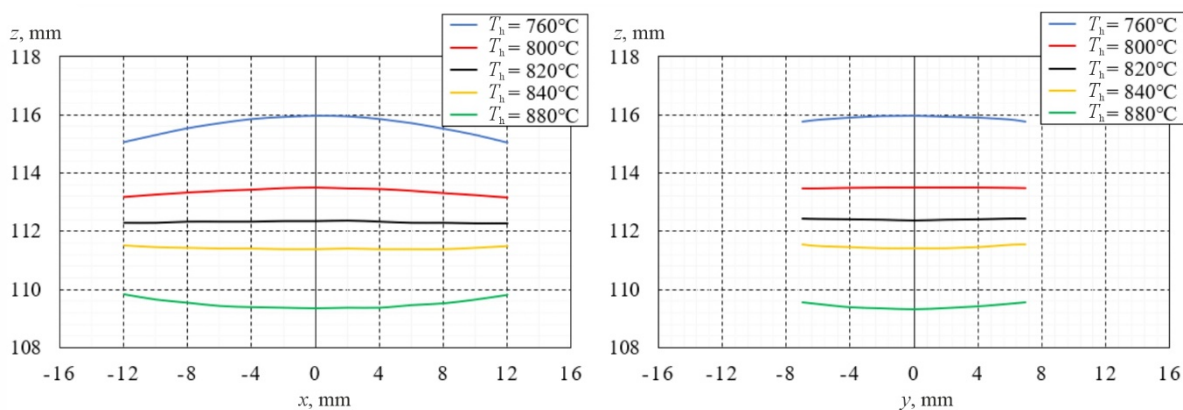


Fig. 11. The shape of crystallization front in sections XZ ($y = 0$) and YZ ($x = 0$) for different heater temperatures T_h (with ingot thickness $h = 14$ mm, container diameter $d = 24$ mm, heater height $h_h = 3d = 72$ mm, cooler height $h_c = 1d = 24$ mm).

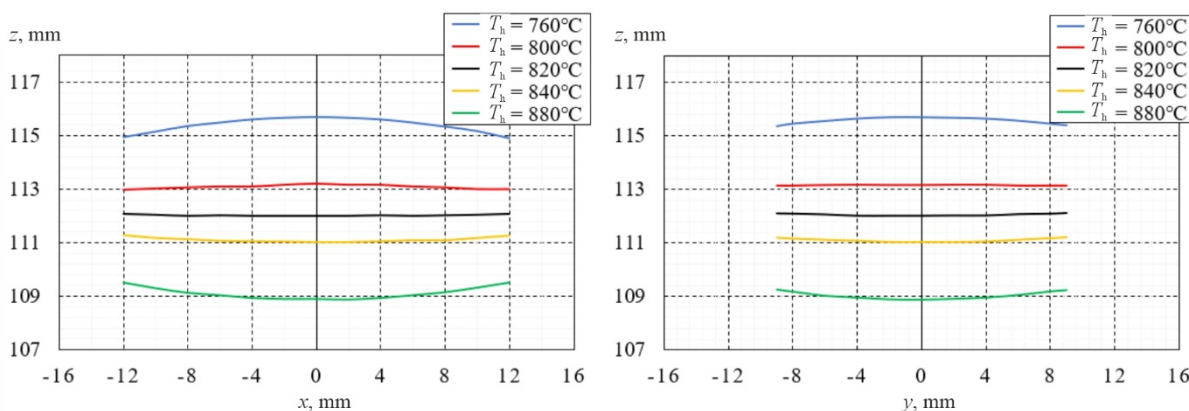


Fig. 12. The shape of crystallization front in sections XZ ($y = 0$) and YZ ($x = 0$) for different heater temperatures T_h (with ingot thickness $h = 18$ mm, container diameter $d = 24$ mm, heater height $h_h = 3d = 72$ mm, cooler height $h_c = 1d = 24$ mm).

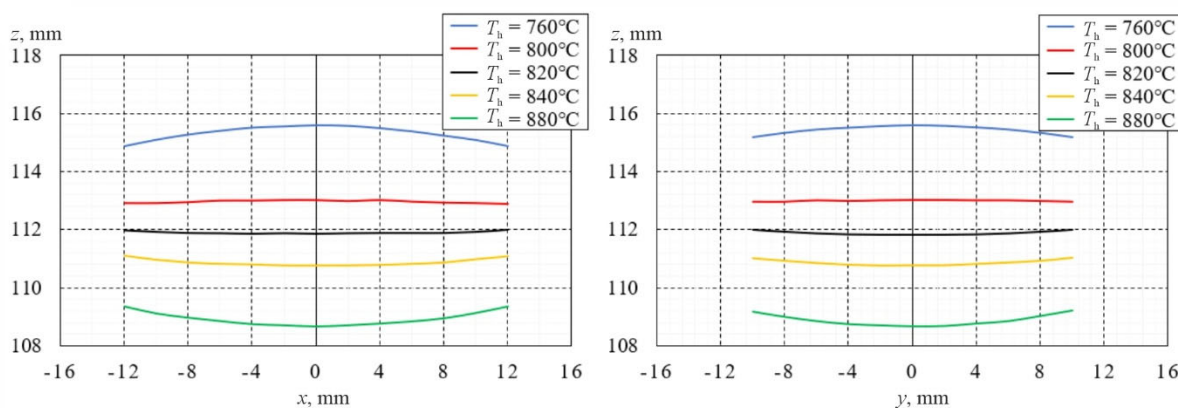


Fig. 13. The shape of crystallization front in sections XZ ($y = 0$) and YZ ($x = 0$) for different heater temperatures T_h (with ingot thickness $h = 20$ mm, container diameter $d = 24$ mm, heater height $h_h = 3d = 72$ mm, cooler height $h_c = 1d = 24$ mm).

As can be seen from Figs. 3 – 13, with an increase in the height of the heater, for a given temperature, the crystallization front is leveled. It can also be seen that at $h_h = 3d$ and $4d$, the crystallization front is flat at the same heater temperature of 820°C , which is optimal for growing a given material, and also conclude that $h_h = 3d$ is the optimal heater parameter. In this case, the optimal height of the coolers is $h_c = 1d$.

Also, based on the simulation results, the yield percentage of material with an improved structure was estimated when using the proposed technology for growing flat ingots depending on the thickness of the ingot h (Fig. 14). Coefficient K is the ratio of the percentage of material with an improved structure for a flat ingot to the percentage of material with an improved structure for a round ingot with the same diameter of the container, growing conditions and the criterion for evaluating the uniformity of the crystallization front.

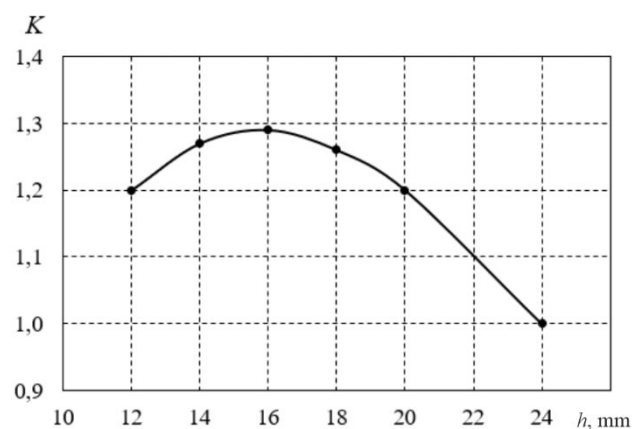


Fig. 14. Coefficient of increase in the yield of material with improved structure when growing flat ingots depending on ingot thickness h .

Therefore, when growing material in the form of flat ingots, the percentage of yield of material with an improved structure is 1.2 – 1.3 times higher compared to growing round ingots in a container of the same diameter. At the same time, the optimal thickness of the ingot for a container with a diameter of 24 mm is a thickness of 15 – 16 mm.

Conclusions

1. The results of computer simulation of the process of manufacturing flat ingots of thermoelectric materials based on Bi_2Te_3 by the method of vertical zone melting are presented. The dependence of the shape of the crystallization front on the geometric dimensions of the heater and coolers, their temperatures, movement speed, and other technological parameters is given.
2. The optimal container geometries, sizes of the heater and coolers, and their temperatures have been determined. It has been shown that with an increase in the heater height at a given temperature, the crystallization front is leveled. It has been established that at a heater temperature of 820°C and coolers of 30°C , the optimal heater height is equal to three container diameters, and the optimal cooler height is equal to one container diameter.
3. It has been shown that growing thermoelectric materials in the form of flat ingots allows increasing the percentage of yield of material with an improved structure by 1.2 – 1.3 times compared to round ingots of the same container diameter.

References

1. *Thermoelectric Modules Market – Global Industry Analysis and Forecast (2023-2029)* / MMR PVT. Ltd, 2023. <https://www.maximizemarketresearch.com/market-report/thermoelectric-modules-mar-ke/2622/>.
2. *Pat. CN216524233U*. Thermoelectric water kettle water level detection circuit. Published 13.05.2022.
3. *Pat. CN105167597B*. A kind of thermo-electric generation hot-water bottle. Published 02.01.2018.
4. *Pat. CN209391675U*. A kind of heating vessel. Published. 17.09.2019.
5. *Pat. CN208806757U*. Thermo-electric generation wild cooker. Published. 30.04.2019.
6. *Pat. GB2605345A*. Cooking vessel. Published 28.09.2022.
7. L.I. Anatyshuk, V.V. Lysko. (2023). On the design of a trench thermoelectric source of heat and electricity. *J. Thermoelectricity*, 1, 93 – 100.
8. Montecucco A., Siviter J. & Knox A.R. (2017). Combined heat and power system for stoves with thermoelectric generators. *Applied Energy*, Elsevier, vol. 185(P2), 1336-1342. DOI: 10.1016/j.apenergy.2015.10.132.
9. Żołądek Maciej, Papis Karolina, Kuś Jakub, Zajac Michal, Figaj Rafał and Rudykh Kyrylo. (2020). The use of thermoelectric generators with home stoves. *E3S Web Conf.*, 173 (2020) 03005. DOI: <https://doi.org/10.1051/e3sconf/202017303005>.
10. *Wood stove thermoelectric generator rabbit ears* [Electronic resource] – Retrieved from: <https://thermoelectric-generator.com/product/wood-stove-thermoelectric-generator-rabbit-ears/>.
11. *45-watt teg generator for wood stoves with air-cooling* [Electronic resource] – Retrieved from: <https://www.tegmart.com/thermoelectric-generators/wood-stove-air-cooled-45w-teg>.
12. *Thermoelectric power generator for fireplace heater* [Electronic resource] – Retrieved from: http://www.thermonamic.com/pro_view.asp?id=828.
13. Cao T., Shi X.L., Li M., Hu B., Chen W., Liu W. Di, Lyu W., MacLeod J., Chen Z.G. (2023). Advances in bismuth-telluride-based thermoelectric devices: progress and challenges. *EScience*, 3(3), Article 100122. <https://doi.org/10.1016/j.esci.2023.100122>.
14. Goldsmid H.J. (2014). Bismuth telluride and its alloys as materials for thermoelectric generation. *Materials*, 7,2577-2592. <https://doi.org/10.3390/ma7042577>.
15. Tritt T. (2000). *Recent trends in thermoelectric materials research, Part Two* (Semiconductors and Semimetals, Volume 70). Academic Press. ISBN-13: 978-0127521794.
16. Lysko V.V., Tudoroi P.F. (2019). Computer simulation of extrusion process of Bi_2Te_3 based tape thermoelectric materials. *J. Thermoelectricity*, 2, 58 – 65.
17. Anatyshuk L.I., Lysko V.V. (2020). *Thermoelectricity: Vol. 5. Metrology of thermoelectric materials*. Chernivtsi: Bukrek. ISBN 978-617-7770-40-3.
18. Anatyshuk L.I., Havrylyuk N.V., Lysko V.V. (2012). Methods and equipment for quality control of thermoelectric materials. *Journal of Electronic Materials*, 41 (6), 1680 – 1685. <https://doi.org/10.1007/s11664-012-1973-1>.
19. Lysko V.V., Nitsovich O.V. (2023). Computer simulation of the process of manufacturing flat ingots of thermoelectric materials based on Bi_2Te_3 by vertical zone melting method. *J. Thermoelectricity*, 3, 18 – 25.
20. COMSOL Multiphysics, v.6.0. www.comsol.com. COMSOL AB, Stockholm, Sweden, 2021.

Submitted: 08.11.2023.

Лисько В.В., канд. фіз.-мат. наук^{1,2}
Ніцович О.В., канд. фіз.-мат. наук¹

¹ Інститут термоелектрики НАН та МОН України,
вул. Науки, 1, Чернівці, 58029, Україна;

² Чернівецький національний університет імені Юрія Федьковича,
вул. Коцюбинського 2, Чернівці, 58012, Україна
e-mail: anatyuch@gmail.com

КОМП'ЮТЕРНА ОПТИМІЗАЦІЯ МЕТОДУ ВЕРТИКАЛЬНОЇ ЗОННОЇ ПЛАВКИ ДЛЯ ВИГОТОВЛЕННЯ ПЛОСКИХ ЗЛИТКІВ ТЕРМОЕЛЕКТРИЧНИХ МАТЕРІАЛІВ НА ОСНОВІ Bi_2Te_3

Представлено результати комп'ютерного моделювання процесу виготовлення плоских злитків термоелектричних матеріалів на основі Bi_2Te_3 методом вертикальної зонної плавки. Наведено залежності форми фронту кристалізації від геометричних розмірів нагрівника та холодильників, їх температур, швидкості руху та інших технологічних параметрів. Проведено багатофакторну комп'ютерну оптимізацію технологічних режимів та конструкції обладнання для вироцування плоских злитків термоелектричних матеріалів на основі Bi_2Te_3 . Бібл. 20, рис. 14.

Ключові слова: моделювання, вертикальна зонна плавка, термоелектричний матеріал, телурид вісмуту.

Література

1. *Thermoelectric Modules Market – Global Industry Analysis and Forecast (2023-2029)* / MMR PVT. Ltd, 2023. <https://www.maximizemarketresearch.com/market-report/thermoelectric-modules-mar-ket/2622/>.
2. *Pat. CN216524233U*. Thermoelectric water kettle water level detection circuit. Published 13.05.2022.
3. *Pat. CN105167597B*. A kind of thermo-electric generation hot-water bottle. Published 02.01.2018.
4. *Pat. CN209391675U*. A kind of heating vessel. Published. 17.09.2019.
5. *Pat. CN208806757U*. Thermo-electric generation wild cooker. Published. 30.04.2019.
6. *Pat. GB2605345A*. Cooking vessel. Published 28.09.2022.
7. L.I. Anatyuchuk, V.V. Lysko. (2023). On the design of a trench thermoelectric source of heat and electricity. *J. Thermoelectricity*, 1, 93 – 100.
8. Montecucco A., Siviter J. & Knox A.R. (2017). Combined heat and power system for stoves with thermoelectric generators. *Applied Energy*, Elsevier, vol. 185(P2), 1336-1342. DOI: 10.1016/j.apenergy.2015.10.132.
9. Żołądek Maciej, Papis Karolina, Kuś Jakub, Zając Michał, Figaj Rafał and Rudykh Kyrylo. (2020). The use of thermoelectric generators with home stoves. *E3S Web Conf.*, 173 (2020) 03005. DOI: <https://doi.org/10.1051/e3sconf/202017303005>.
10. *Wood stove thermoelectric generator rabbit ears* [Electronic resource] – Retrieved from: <https://thermoelectric-generator.com/product/wood-stove-thermoelectric-generator-rabbit-ears/>.

11. 45-watt teg generator for wood stoves with air-cooling [Electronic resource] – Retrieved from: <https://www.tegmart.com/thermoelectric-generators/wood-stove-air-cooled-45w-teg>.
12. Thermoelectric power generator for fireplace heater [Electronic resource] – Retrieved from: http://www.thermonamic.com/pro_view.asp?id=828.
13. Cao T., Shi X.L., Li M., Hu B., Chen W., Liu W. Di, Lyu W., MacLeod J., Chen Z.G. (2023). Advances in bismuth-telluride-based thermoelectric devices: progress and challenges. *EScience*, 3(3), Article 100122. <https://doi.org/0.1016/j.esci.2023.100122>.
14. Goldsmid H.J. (2014). Bismuth telluride and its alloys as materials for thermoelectric generation. *Materials*, 7,2577-2592. <https://doi.org/10.3390/ma7042577>.
15. Tritt T. (2000). *Recent trends in thermoelectric materials research, Part Two* (Semiconductors and Semimetals, Volume 70). Academic Press. ISBN-13: 978-0127521794.
16. Lysko V.V., Tudoroi P.F. (2019). Computer simulation of extrusion process of Bi_2Te_3 based tape thermoelectric materials. *J. Thermoelectricity*, 2, 58 – 65.
17. Anatyshuk L.I., Lysko V.V. (2020). *Thermoelectricity: Vol. 5. Metrology of thermoelectric materials*. Chernivtsi: Bukrek. ISBN 978-617-7770-40-3.
18. Anatyshuk L.I., Havrylyuk N.V., Lysko V.V. (2012). Methods and equipment for quality control of thermoelectric materials. *Journal of Electronic Materials*, 41 (6), 1680 – 1685. <https://doi.org/10.1007/s11664-012-1973-1>.
19. Lysko V.V., Nitsovich O.V. (2023). Computer simulation of the process of manufacturing flat ingots of thermoelectric materials based on Bi_2Te_3 by vertical zone melting method. *J. Thermoelectricity*, 3, 18 – 25.
20. COMSOL Multiphysics, v.6.0.www.comsol.com. COMSOL AB, Stockholm, Sweden, 2021.

Надійшла до редакції: 08.11.2023.